UNMIXING INTIMATE MIXTURES USING BÉZIER SURFACES

Bikram Koirala[1] Behnood Rasti[2], Zakaria Bnoulkacem[1], Paul Scheunders[1]

[1] Imec-Visionlab, University of Antwerp (CDE) Universiteitsplein 1, B-2610 Antwerp
[2] Helmholtz-Zentrum Dresden-Rossendorf (HZDR), Helmholtz Institute Freiberg for Resource Technology.

ABSTRACT

Due to the complex interaction of incident light with intimately mixed materials, the relationship between acquired reflectance spectra and the composition of materials is highly nonlinear. Spectral variability due to changes in illumination and acquisition conditions further complicates the unmixing procedure. In this work, we propose a method to accurately characterize a nonlinear simplex by a Bézier surface, by utilizing training samples. The fractional abundances of a test sample can be estimated by reconstruction of its reflectance spectrum on the Bézier surface. Moreover, the proposed method is made invariant to changes in the acquisition and illumination conditions. Experiments are conducted on simulated and real laboratory-generated mineral powder mixtures. The experimental results confirm the potential of the proposed methodology.

Index Terms— Hyperspectral image, nonlinear unmixing, intimate mixtures

1. INTRODUCTION

Hyperspectral unmixing techniques estimate the fractional abundances of the different materials contained within the field of view of a pixel by minimizing the error between the measured spectral reflectance and the spectrum that a particular mixing model generates. The most popular mixing model in the remote sensing community is the linear mixing model (LMM). The LMM assumes that any incident ray of light interacts with a single pure material in the pixel instantaneous field of view before reaching the sensor. By considering the physical non-negativity and sum to one constraint of the fractional abundances, the Fully Constrained Least Squares Unmixing procedure (FCLSU) was proposed [1].

As the interaction of light with the Earth's surface is very complex, nonlinear unmixing models have been developed [2, 3]. Bilinear mixing models (e.g., PPNM [4]) assume that an incident ray of light interacts with two pure materials before reaching the sensor. To explain higher-order interactions, multilinear mixing models (e.g., [5]) and intimate mixture models (e.g., [6, 7]) have been developed.

Some attempts have been made to learn the nonlinearity of a dataset by applying supervised machine learning [8, 9, 10, 11]. For example, in [10, 11], a mapping between the actual nonlinear spectra and linearly mixed spectra was learned by utilizing training samples. The FCLSU procedure can then be applied to obtain the fractional abundances of test samples. A major disadvantage of these supervised methods is the lack of generalizability [12]. The trained model does not perform well on test samples when the training and test samples lie on different data manifolds. This occurs due to the variability of the acquired datasets, caused by changes in acquisition and illumination conditions [12]. To tackle both nonlinearity and spectral variability, we developed a robust supervised unmixing method for nonlinear hyperspectral unmixing of binary mixtures [12].

In this work, we design a framework that is suitable to accurately characterize higher dimensional ($2 <$ the number of pure material) nonlinear data manifolds. The method assumes that any nonlinear data manifold can be reconstructed by utilizing a Bézier surface of a certain degree. To reconstruct a Bézier surface, training samples in the form of control points are required. Estimating the fractional abundances of test samples then boils down to minimizing the reconstruction error between the input spectrum and the Bézier surface. To tackle the spectral variability, a transformation function between the training and test data manifolds is learned by utilizing the spectral reflectance of the pure materials (endmembers). To validate our strategy, we produced a hyperspectral data set of 36 different clay powder mixtures. To introduce spectral variability, each sample was acquired by two different sensors: an ASD spectroradiometer and a snapscan shortwave infrared (SWIR) hyperspectral camera.

2. HYPERSPECTRAL DATA MODELING USING A BÉZIER SURFACE

2.1. characterization of nonlinear data manifolds

In [12], we have developed a method for accurately estimating the composition of binary powder mixtures that combines spectral mixture modeling [13] with machine learning. This method was further improved in [14]. This method assumes that a data manifold sampled by a number of binary mixtures with varying compositions is a curve in spectral space between the two pure minerals. The relative arc length be-

tween a mixture and the two endmembers can be regarded as a proxy for its fractional abundances, the relation between both is obtained by machine learning.

In order to make the methodology in [14] applicable to mixtures of more than two materials, we require a framework that can accurately characterize higher dimensional nonlinear simplices. For this, we will utilize the properties of higher dimensional Bézier surfaces. A Bézier surface is a nonlinear surface that can be reconstructed by interpolation of a number of control points. A general n^{th} order Bézier surface has $\frac{(n+p-1)!}{n!\,(p-1)!}$ control points, where p denotes the number of endmembers. As an example, take ternary mixtures, for which the Bézier surface is defined as:

$$\mathbf{y} = \sum_{\substack{i+j+k=n,\\ i,j,k\geq 0}} \frac{n!}{i!\,j!\,k!} a_1^i a_2^j a_3^j \alpha^i \beta^j \gamma^k \qquad (1)$$

where $\mathbf{y}$ is the spectrum of a test sample with $\mathbf{a} = \begin{bmatrix} a_1 \\ a_2 \\ a_3 \end{bmatrix}$ its fractional abundances. The fractional abundances obey both the non-negative constraint and the sum-to-one constraint. $\alpha^i \beta^j \gamma^k$ describes control points. The higher the value of n, the better the reconstruction. In Fig. 1, we depict the fractional abundances of the control points with a Bézier surface of order $n = 7$. As can be observed, the fractional abundances of the control points uniformly cover the probability simplex. Estimating the fractional abundances of any test sample then boils down to minimization of reconstruction error between the input spectrum and the spectrum generated by applying Eq. (1).

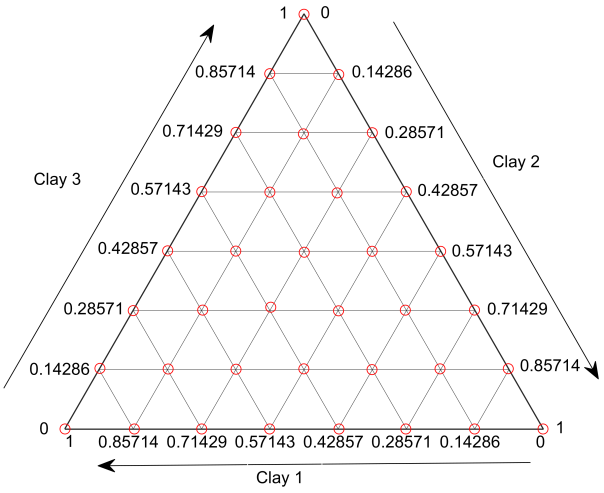

Fig. 1. The ternary diagram of three material mixtures.

Although this approach can characterize the nonlinearity of a hyperspectral dataset accurately, it suffers from spectral variability caused by variations in the illumination conditions and acquisition conditions.

2.2. Tackling spectral variability

Random scaling effects caused by illumination variations can be removed by projecting all spectra onto the unit hypersphere (i.e., dividing the spectra by their length). A manifold is transformable to other environmental and acquisition conditions. As an example, think of mixtures of the same pure materials, measured by another sensor, for which the spectra will lie on a different manifold. When we assume that these two data manifolds are linearly related, the new manifold can be transformed into the original one. For this, we require the endmember spectra and the incenter of both manifolds. First, the arc lengths between the corresponding endmember pairs are calculated. On the unit hypersphere, the arc length between any two spectra is simply given by the angle between them and can be computed by just calculating the arc cosine of their dot product. Additionally, the arc length between endmembers and the incenters is required. The incenters of the manifolds are obtained by utilizing the methodology proposed in [15]. From these arc lengths, a transformation matrix between the two manifolds can be calculated that includes translation, rotation, and scaling.

To determine the fractional abundance of a test mixture, first, the arc lengths between the mixture and the endmembers are determined. Then, these arc lengths are transformed into the original trained manifold. Finally, the spectrum for which the arc lengths match those of the mixture is constructed on the Bézier surface, and its corresponding fractional abundances are obtained by inverting Eq. (1). In this work, the proposed methodology will be denoted by Bézier supervised unmixing (**BSU**).

3. EXPERIMENTS

3.1. The Data

3.1.1. Simulated Data

To demonstrate that Bézier surfaces can accurately characterize nonlinear data manifolds, we simulated a Hapke dataset (see Figure 2 (b)) by constructing spectral mixtures of three homogeneous clay powders that follow the Hapke model [6]. The spectral reflectance of three pure clay powders, i.e., Kaolin, roof clay, and calcium hydroxide ($Ca(OH)_2$) are acquired by an ASD spectroradiometer and used as endmembers (see Fig. 2(a)). The ASD spectroradiometer generates spectra of 2151 bands, ranging from 350 nm to 2500 nm with a step size of 1 nm. 1036 spectra were generated with uniformly and randomly distributed fractional abundances. 36 uniformly sampled spectra ($n = 7$) will be used as control points (see red circles in Figure 2(b)). We refer to this dataset as the spectroradiometer-simulated dataset. Similarly, we simulated a Hapke dataset by acquiring the clay powders with a hyperspectral snapscan camera (IMEC), generating spectra of 100 bands, ranging from 1120 nm to 1675 nm.

We refer to this dataset as the camera-simulated dataset (see Figure 2(c)). In both datasets, each spectrum was multiplied by a random factor between 0.5 and 2 to introduce variability due to changes in the acquisition and illumination angles.

3.1.2. Real Data

We prepared 36 samples by homogeneously mixing three clay powders (Kaolin, roof clay, and calcium hydroxide). All possible combinations of these powders were considered, i.e., 3 pure clay powders, 3 binary combinations (Kaolin-roof clay, Kaolin-calcium hydroxide, Roof clay-calcium hydroxide), and 1 ternary combination (Kaolin-roof clay-calcium hydroxide). Within each clay combination, samples with different mixture fractions are generated so that the ground truth fractional abundances uniformly cover the three-dimensional simplex, with a step size of 14.286 % mass ratios. In this way, 6 unique mixtures are generated for each binary clay combination and 15 for the ternary clay combination, making a total of 33 mixtures. These mixtures correspond to the required control points for a Bézier surface of order $n = 7$ (see Fig. 1). The three pure clay powders occupy the corners of the simplex, all binary mixtures lie on the lines connecting two powders while the ternary mixtures lie inside the simplex.

Mixtures were produced by weighing and combining the pure components. For each sample, we fixed the total weight to 10 g (precision of scale 0.001 g). To produce a homogeneous mixture, each 10 g sample was put inside a glass bottle that was rotated continuously for five minutes. Using the particle densities of the pure clays, we converted the weight to volume fraction by:

$$a_j = \frac{\frac{M_j}{\rho_j}}{\sum_{j=1}^{p} \frac{M_j}{\rho_j}}, \tag{2}$$

where p denotes number of pure materials, M_j is the mass fraction of component j, and ρ_j its density. These samples were further put inside a clear plastic jar with an interior diameter of 3.048 cm and a height of 1.524 cm. Approximately 3 g of the mixtures was required to fill the sample holder. These samples were further compacted and smoothened using a stamp compactor.

The spectral reflectances of these samples were acquired by two different hyperspectral sensors: an ASD spectroradiometer and a SWIR hyperspectral camera. Although the original frame size of the raw images acquired by the hyperspectral camera was 150×150 pixels, we manually clipped 70×70 pixels from the center of the images to remove the edge of the sample holders. Since no spatial variation between the spectra was observed, the mean spectrum of the clipped image was considered for further analysis.

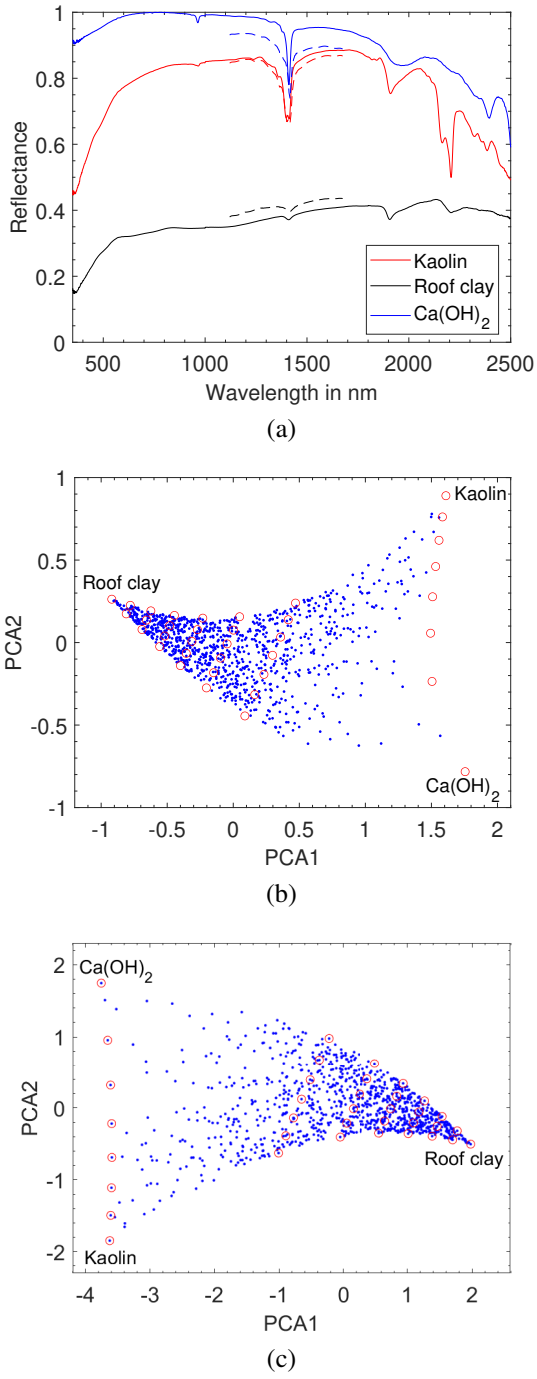

Fig. 2. (a) Spectral reflectance of pure clay powders (end-members) acquired by the ASD spectroradiometer (full line) and the hyperspectral camera (dashed); (b) PCA reduced Hapke data manifold (spectroradiometer-simulated dataset). ; (c) PCA reduced Hapke data manifold (camera-simulated dataset). Here blue dots denote the nonlinearly mixed data, and red circles denote the control points.

3.2. Experimental Setup

The following unmixing methods were used as competing methods in the experiments: Linear unmixing: FCLSU [1], Bilinear unmixing: PPNM [4], Multilinear unmixing: MLM [5] and the Hapke model [6]. For these four methods, the utilized endmembers are the ones, acquired by the hyperspectral sensors. For the binary mixtures, the Robust supervised unmixing method (**RSM**) ([14]) is applied, using training samples obtained from one out of two sens ors.

All quantitative comparisons are provided by the abundance root mean squared error (RMSE), i.e. the error between the estimated fractional abundances ($\hat{\mathbf{A}}$) and the ground truth fractional abundances ($\mathbf{A}$):

$$\text{Abundance RMSE} = \sqrt{\frac{1}{pm}\sum_{k=1}^{p}\sum_{i=1}^{m}\left(\hat{\mathbf{A}}_{ki} - \mathbf{A}_{ki}\right)^2} \times 100 \tag{3}$$

where p and m denote the number of endmembers and the number of mixed spectra respectively.

3.3. Unmixing Experiments

3.3.1. Simulated Dataset

To demonstrate that our method can accurately characterize nonlinear manifolds and transform one manifold onto another, in Fig. 3, we show the control points (black dots) obtained from the spectroradiometer-simulated dataset and the transformed control points (red circles) of the camera-simulated dataset. In general, the transformed control points lie close to the true control points. A relatively large error for some control points (binary mixtures of Kaolin and Calcium hydroxide) indicates that the Hapke model is highly sensitive to the reflectance values of the material. In particular, the spectra of $Ca(OH)_2$ from the spectrometer and camera are quite different (see Fig. 2(a)).

Table 1 shows the abundance root mean squared error for all unmixing methods applied to the camera-simulated dataset (see Section 3.1.1). For both RSM and BSU, training samples (control points) were obtained from the spectroradiometer-simulated dataset. To match the spectral range of the spectroradiometer and the camera-simulated datasets, unmixing methods were applied only using the wavelength region [1120 - 1675 nm]. Because RSM can be applied only on binary mixtures, the performance of all unmixing methods on binary mixtures is shown separately. As can be observed, the Hapke model accurately estimated the fractional abundances from the camera-simulated dataset, when no random scaling is introduced. This is because the Hapke model was used to simulate this dataset. Neither linear nor bilinear/multilinear mixing models could perform well, suggesting that these models are not suitable to characterize the nonlinearity of intimate mixtures. When random scaling was introduced, the Hapke model fails and the other mixing models perform worse than

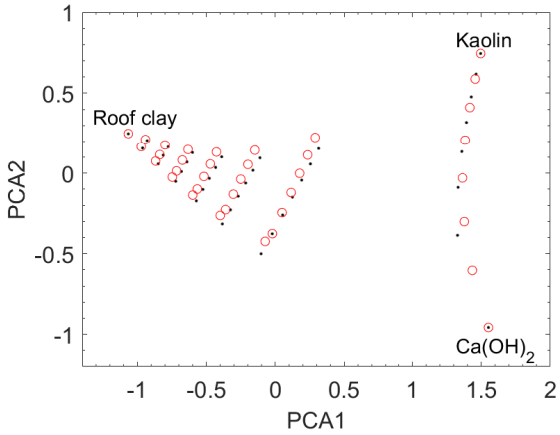

Fig. 3. PCA reduced Hapke data manifold. Here black dots denote the control points obtained from the spectroradiometer-simulated dataset while the red circles denote the transformed control points of the camera-simulated dataset.

without scaling, showing that none of the unmixing models are invariant to spectral variability. RSM was the best performer (see Table 1 (with random scaling)) for the binary mixtures while BSU outperformed others on the ternary mixtures.

Table 1. RMSE (Camera-simulated dataset). The best performances are shown in bold.

	FCLSU	PPNM	MLM	Hapke	RSM	**BSU**
Binary mixtures (no random scaling)	20.55	30.21	20.55	**0.00**	4.46	5.12
Binary mixtures (with random scaling)	48.82	36.36	46.33	49.09	**4.46**	5.12
Ternary mixtures (no random scaling)	21.05	35.50	21.05	**0.03**	-	5.99
Ternary mixtures (with random scaling)	39.26	36.44	36.85	42.13	-	**5.99**

3.3.2. Real Dataset

In the final experiment, we applied the proposed method to the real dataset acquired by the IMEC hyperspectral camera (see Section 3.1.2). For both RSM and BSU, training samples were obtained from the spectroradiometer dataset. As can be observed from Table 2, except for RSM and BSU, none of the unmixing methods could perform well for this dataset. The main reason for the lower performance of the Hapke model is that the mineral particles in these mixtures are non-spherically shaped and behave as anisotropic scatterers. Similar to the simulated dataset, RSM outperformed others for binary mixtures while BSU was the best performer for estimating the fractional abundances of ternary mixtures.

Table 2. RMSE (Real dataset acquired by the IMEC hyperspectral camera). The best performances are shown in bold.

	FCLSU	PPNM	MLM	Hapke	RSM	**BSU**
Binary mixtures	11.52	16.89	11.46	12.68	**2.63**	2.89
Ternary mixtures	11.08	18.19	11.05	14.01	-	**4.08**

4. CONCLUSIONS

In this work, we proposed a method to accurately estimate the composition of intimately mixed samples. Moreover, the proposed method is made invariant to spectral variability, caused by changes in the acquisition and illumination conditions. The proposed method was validated on a simulated dataset and a dataset generated in laboratory settings and in cross-sensor situations. In future work, we will validate the proposed method on a multisensor hyperspectral benchmark dataset that we recently generated.

5. REFERENCES

[1] J. W. Boardman, "Geometric mixture analysis of imaging spectrometry data," in *IEEE International Geoscience and Remote Sensing Symposium*, 1994, pp. 2369–2371.

[2] R. Heylen, M. Parente, and P. Gader, "A review of nonlinear hyperspectral unmixing methods," *IEEE Journal of Selected Topics in Applied Earth Observations and Remote Sensing*, vol. 7, no. 6, pp. 1844–1868, 2014.

[3] N. Dobigeon, J.Y. Tourneret, C. Richard, Jose Carlos M. Bermudez, Stephen McLaughlin, and Alfred O. Hero, "Nonlinear unmixing of hyperspectral images," *IEEE Signal Processing Magazine*, vol. 31, no. 1, pp. 82–94, JAN 2014.

[4] Y. Altmann, A. Halimi, N. Dobigeon, and J. Tourneret, "Supervised nonlinear spectral unmixing using a post-nonlinear mixing model for hyperspectral imagery," *IEEE Transactions on Image Processing*, vol. 21, no. 6, pp. 3017–3025, 2012.

[5] R. Heylen and P. Scheunders, "A multilinear mixing model for nonlinear spectral unmixing," *IEEE Transactions on Geoscience and Remote Sensing*, vol. 54, no. 1, pp. 240–251, Jan 2016.

[6] B. Hapke, "Bidirectional reflectance spectroscopy: 1. theory," *Journal of Geophysical research*, vol. 86, pp. 3039–3054, 1981.

[7] B. Rasti, B. Koirala, and P. Scheunders, "Hapkecnn: Blind nonlinear unmixing for intimate mixtures using hapke model and convolutional neural network," *IEEE Transactions on Geoscience and Remote Sensing*, vol. 60, pp. 1–15, 2022.

[8] G. M. Foody, "Relating the land-cover composition of mixed pixels to artificial neural network classification outpout," *Photogrammetric Engineering and Remote Sensing*, vol. 62, pp. 491–499, 1996.

[9] G. Licciardi and F. D. Frate, "Pixel unmixing in hyperspectral data by means of neural networks," *IEEE Transactions on Geoscience and Remote Sensing*, vol. 49, pp. 4163–4172, 2011.

[10] B. Koirala, R. Heylen, and P. Scheunders, "A neural network method for nonlinear hyperspectral unmixing," in *IEEE International Geoscience and Remote Sensing Symposium*, 2018, pp. 4233–4236.

[11] B. Koirala, M. Khodadadzadeh, C. Contreras, Z. Zahiri, R. Gloaguen, and P. Scheunders, "A supervised method for nonlinear hyperspectral unmixing," *Remote Sensing*, vol. 11, no. 20, 2019.

[12] B. Koirala, Z. Zahiri, A. Lamberti, and P. Scheunders, "Robust supervised method for nonlinear spectral unmixing accounting for endmember variability," *IEEE Transactions on Geoscience and Remote Sensing*, vol. 59, no. 9, pp. 7434–7448, 2021.

[13] R. Heylen, D. Burazerovic, and P. Scheunders, "Nonlinear spectral unmixing by geodesic simplex volume maximization," *IEEE Journal of Selected Topics in Signal Processing*, vol. 5, no. 3, pp. 534–542, 2011.

[14] B. Koirala, Z. Zahiri, and P. Scheunders, "A robust supervised method for estimating soil moisture content from spectral reflectance," *IEEE Transactions on Geoscience and Remote Sensing*, vol. 60, pp. 1–13, 2022.

[15] R. Heylen and P. Scheunders, "A distance geometric framework for nonlinear hyperspectral unmixing," *IEEE Journal of Selected Topics in Applied Earth Observations and Remote Sensing*, vol. 7, no. 6, pp. 1879–1888, 2014.